Reaction $K^-p \to \bar{K}^0 p\pi^-$ at 6.5 GeV/c

S. Toaff,* B. Musgrave, J. J. Phelan,† P. Schultz, R. Smith, and A. J. Snyder‡
Argonne National Laboratory, Argonne, Illinois 60439

R. Ammar, R. Davis, C. Eklund,§ L. Herder, N. Kwak, L. Loos,‖ R. Riemer, and R. Stump
University of Kansas, Lawrence, Kansas 66045

(Received 22 July 1980)

Data from the ANL 12-foot bubble chamber have been used to study the $\bar{K}^0\pi^-$ system in the reaction $K^-p \to \bar{K}^0 p\pi^-$ at 6.5 GeV/c. Signals for the production of $K^*(892)$, $K^*(1430)$, and $K^*(1780)$ were observed with cross sections of 181 ± 22, 41.2 ± 6, and 8.4 ± 2.9 μb, respectively. The partial waves contributing to the production of the $\bar{K}^0\pi^-$ system from threshold up to 1.7 GeV were studied. The principal conclusions are: (i) $K^*(892)$ and $K^*(1430)$ production is dominated by natural-parity exchange, (ii) the ratio of unnatural- to natural-parity exchange increases with the resonance mass, consistent with the predictions of a triple-Regge model, (iii) there is evidence for a broad 0^+ s-wave enhancement, with considerable s-d and s-p interference, centered at 1.2 GeV, and (iv) the $m = 2$ amplitudes are negligible.

I. INTRODUCTION

The single-pion-production channels in K^--proton interactions

$$K^-p \to \bar{K}^0 p\pi^-, \tag{1a}$$

$$K^-p \to K^-p\pi^0, \tag{1b}$$

$$K^-p \to K^-\pi^+n \tag{1c}$$

have been extensively studied up to momenta as high as 16 GeV/c. Below a mass of 1.5 GeV, the $(K\pi)$ system is dominated by production of the $K^*(892)$ with $J^P = 1^-$ and $K^*(1430)$ with $J^P = 2^+$. A complete understanding of the production mechanism for such $K\pi$ states involves study of both the non-charge-exchange reactions (1a) and (1b) and the charge-exchange process (1c).

A bubble-chamber study of the charge-exchange reaction obtained a good description of $K^*(892)$ production assuming ρ-A_2 natural-parity exchange combined with absorbed π-B unnatural-parity exchange.[1] Subsequent spectrometer experiments confirmed and extended these ideas.[2] The non-charge-exchange reaction (1a) has been extensively studied, most recently in a high-statistics experiment at 4.2 GeV/c,[3] with the conclusion that natural-parity (ω, f) exchanges are dominant in the production of both $K^*(892)$ and $K^*(1430)$ resonances. The s-wave production of $K\pi$ is an important consideration in describing the $K\pi$ system up to a mass of 1.5 GeV.

In this paper, we report results of a study of the reaction $K^-p \to \bar{K}^0 p\pi^-$ at 6.52 GeV/c which come from a large, million-picture exposure of the Argonne 12-ft. hydrogen bubble chamber. Some results from this exposure have already been published.[4,5] Both K^* resonances are studied and the partial cross sections for natural- and unnatural-parity exchange are separated. We also present results of a partial-wave analysis of the $\bar{K}^0\pi^-$ system. The cross section for 0^+ exchange is extracted and results are compared with those from previous analyses at higher energies.

II. EXPERIMENTAL DETAILS

The data come from an exposure of the ANL 12-ft. bubble chamber to a rf-separated K^- beam of 6.52 GeV/c. The beam had a momentum spread of $\pm 1\%$ and a contamination of about 5% π^- and $<25\%$ μ^-. A total of about one million pictures were taken and events belonging to the two-prong $+V$ topology were studied. The data presented here come from an analysis of about 65% of the film.

In order to determine the K^- flux, we also analyzed events belonging to the three-prong topology. This topology contains events representing the decay $K^- \to \pi^-\pi^-\pi^+$ as well as background events representing the diffraction process $K^-p \to K^-\pi^+\pi^-p$ in which the proton track is too short to be seen. A Monte Carlo study of artificially generated diffractive events showed that less than 1% of them would successfully fit the K^- decay hypothesis, and so all fits to the decay hypothesis were interpreted as genuine $K^- \to \pi^-\pi^-\pi^+$ events. There were 6100 such events.

The scanning efficiency was determined from a rescan of about 13% of the film. Table I presents the results for each of the topologies of interest, namely three-prong events ($C3$), two-prong $+V$ events ($C2V$), as well as a similar topology in which the scanner could not decide whether the neutral was a V or a γ and classified it as ambiguous ($C2A$). The scanning efficiency for $C2A$ events is seen to be about 30% smaller than for the $C2V$ events. However, kinematic analysis of the $C2A$

TABLE I. Scanning efficiencies.

Topology	Single-scan efficiency	Overall scan efficiency (13% rescan)
$C2V$	0.810 ± 0.003	0.826 ± 0.002
$C2A$	0.549 ± 0.009	0.576 ± 0.008
$C3$	0.730 ± 0.010	0.750 ± 0.009

events subsequently revealed that only about 20% of them belonged to the $C2V$ category and that these have a scan efficiency of only about $(6 \pm 4)\%$ lower than that for events originally classified as $C2V$.

Events were measured on the automated measuring machine POLLY at Argonne and on conventional measuring machines at Kansas. The measurements were processed using the geometrical-reconstruction program TVGP and the kinematic-fitting program SQUAW. The number of successful fits obtained needs to be corrected for a variety of losses that affect the original sample of found events. These include the occurrence of genuine but unmeasurable events, losses due to events failing TVGP, the failure of SQUAW to fit bona fide events, and various other factors. Table II presents the ratio R of the number of events giving a V or $K^- \to \pi^-\pi^-\pi^+$ fit to the number of events found, for each of the topologies of interest.

There is a significant loss of events in which the V decays close to the production vertex, such events being frequently misinterpreted as four-prong events. In order to eliminate this bias, we excluded events where the V traveled less than 0.8 cm before decaying. We also excluded events with V decays occurring outside the fiducial volume or more than 60 cm from the production vertex. Appropriate potential-length weighting factors were applied to each event to correct for the effect of these cuts. The average weighting factor for K_S^0 events was 1.13.

From a knowledge of the scanning efficiencies, the ratio R, and the K^- flux (determined from the number of $K^- \to \pi^-\pi^-\pi^+$ decays and the branching ratio for this decay mode), we find the cross-section basis to be 22.7 ± 2.4 events/μb uncorrected for neutral decays of K_S^0. Additional corrections need to be applied for the various cuts described later.

TABLE II. Ratio of number of events given a V or $K^- \to \pi^-\pi^-\pi^+$ fit to the number of events found.

Topology	Ratio
$C2V$	0.631
$C2A$	0.124
$C3$	0.565

There were approximately 35 800 events where the V gave a unique three-constraint K_S^0 fit and about 22 400 events yielding a unique three-constraint Λ fit. There were an insignificant number of events that fit both the K_S^0 and γ hypotheses, but about 8200 events gave fits to both K_S^0 and Λ. In all these three-constraint fits, the V was required to point to the production vertex, but no other production information was used. Detailed studies showed that only about 4% of all K_S^0 events (or about 1500 events) are contained in the ambiguous sample.[5]

The events selected for study in this paper are seven-constraint multivertex fits to reaction (1a). If events having a K_S^0/Λ ambiguity gave a seven-constraint fit to (1a) but did not have a seven-constraint fit to a hypothesis in which the V fits a Λ, then the higher constraint K_S^0 interpretation was accepted. In those cases where the highest constraint classes yielding K_S^0 and Λ fits, respectively, were the same, the K_S^0/Λ ambiguity was resolved on the basis of the χ^2 probability ratio for the two fits. We estimate that our K_S^0 event sample, selected in this manner, has less than 0.4% Λ contamination.

Additional experimental details may be found in Ref. 5.

III. MAIN FEATURES OF THE REACTION $K^- p \to \bar{K}^0 p \pi^-$

To minimize ambiguities between different possible kinematic channels with a $\bar{K}^0$, we require that events belonging to the seven-constraint reaction (1a) have the following characteristics:

(a) Overall χ^2 probability greater than 1%. (This resulted in a 7% loss of events since the probability distribution is not flat.)

(b) Missing mass squared lying between -0.05 and 0.05 GeV^2. (This results in an additional 2% loss.)

(c) The seven-constraint fit preferred over all lower-constraint fits.

There were 2850 such weighted events representing reaction (1a). Using our measured cross-section basis and correcting for $\bar{K}^0$ escape losses, as well as losses due to the cuts (a) and (b) discussed above, we find the cross section for reaction (1a) to be 400 ± 42 μb. This is in good agreement with the value obtained by interpolating to our momentum, the published cross sections for this reaction.[6]

Figure 1 shows the Dalitz plot for reaction (1a). There are strong signals for the $K^*(892)$ and $K^*(1430)$ resonances. In Figs. 2(a)–2(c), the three

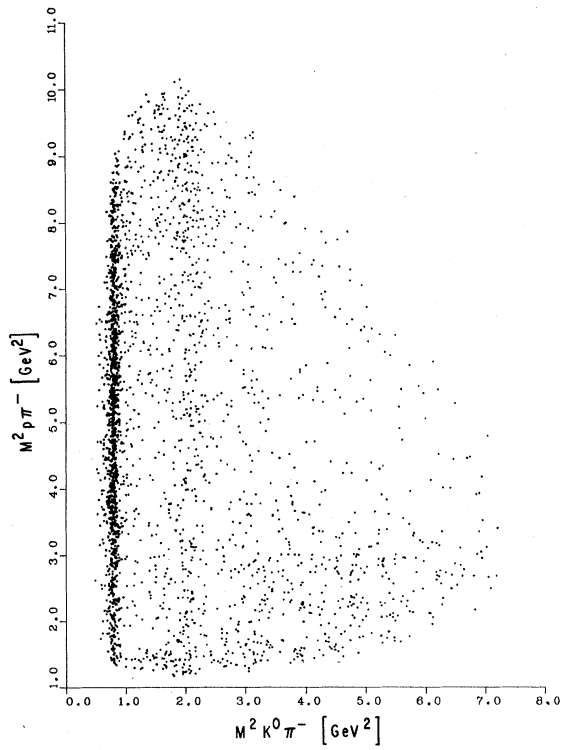

FIG. 1. Dalitz plot for reaction (1a).

different two-body mass combinations are given. Again, the most prominent signals are the $K^*(892)$ and $K^*(1430)$ enhancements with a small bump around the mass of the $K^*(1780)$. The $K^*(892)$ is produced above very low (~10%) background, while the $K^*(1430)$ is produced on relatively high (~50%) background.

We have divided the $\bar{K}^0\pi^-$ effective-mass distribution into 11 mass bins, and Fig. 3 shows the differential cross section $d\sigma/dt'$ for the various mass bins, where $t' = t_{\min} - t$, and t is the four-momentum transfer between the incident K^- and the outgoing $\bar{K}^0\pi^-$ system. The shape of these distributions varies slowly as a function of $M(\bar{K}^0\pi^-)$. We have used the maximum-likelihood method to fit the differential-cross-section distribution in the region $0.1 < t' < 1.0$ (GeV/c)^2 to the form

$$d\sigma/dt' = Ae^{-\alpha t'}. \quad (2)$$

The results are presented in Table III. There is a distinctive change (50%) of the slope parameter α as one goes toward the high-mass bins.

Another distinctive feature of these distributions is a forward dip which tends to disappear at higher masses. This dip, which is pronounced in the $K^*(892)$ region, only appears for the $K^*(1430)$ region after a background subtraction is made (see Fig. 6). Figures 4 and 5 show the polar and azimuthal decay angular distributions in the usual t channel for the $(K^0\pi^-)$ system with the requirement $t' < 1$ GeV$^2/c^2$. The marked characteristics of these distributions are the following:

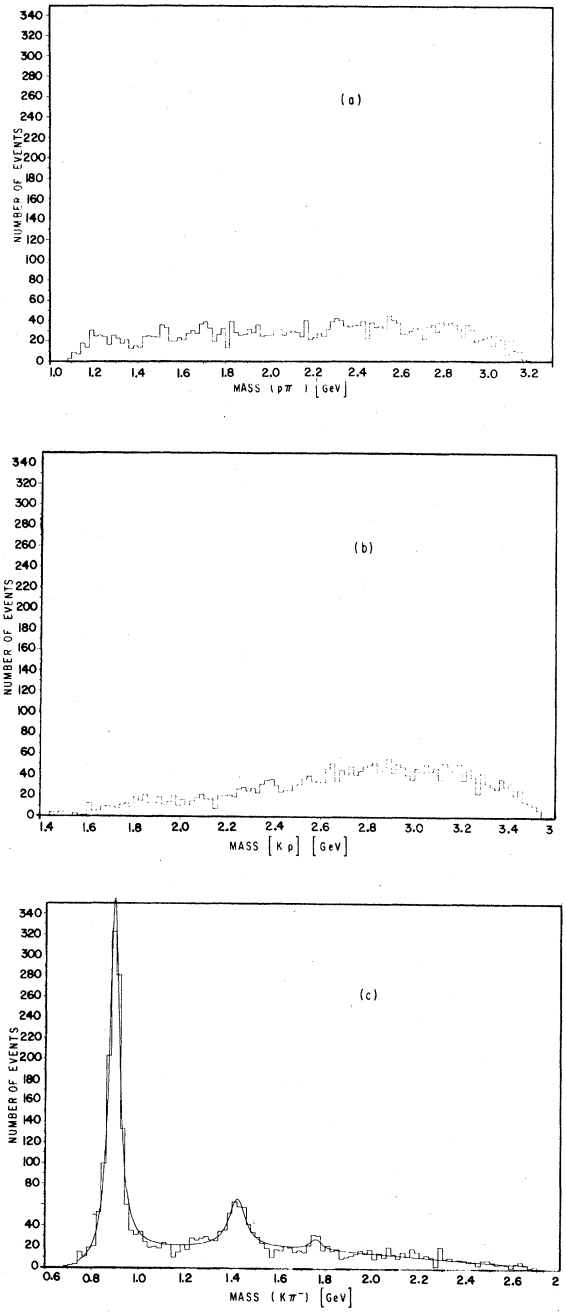

FIG. 2. Effective-mass distributions in the reaction $K^- p \to \bar{K}^0 p\pi^-$. (a) $M(p\pi^-)$, (b) $M(\bar{K}^0 p)$, and (c) $M(\bar{K}^0\pi^-)$. The solid line represents the results of the fit described in the text.

(a) There is a continuous change in the distribution in polar angle θ_t, from a behavior of $\cos^2\theta_t$ to a more complicated structure as the effective

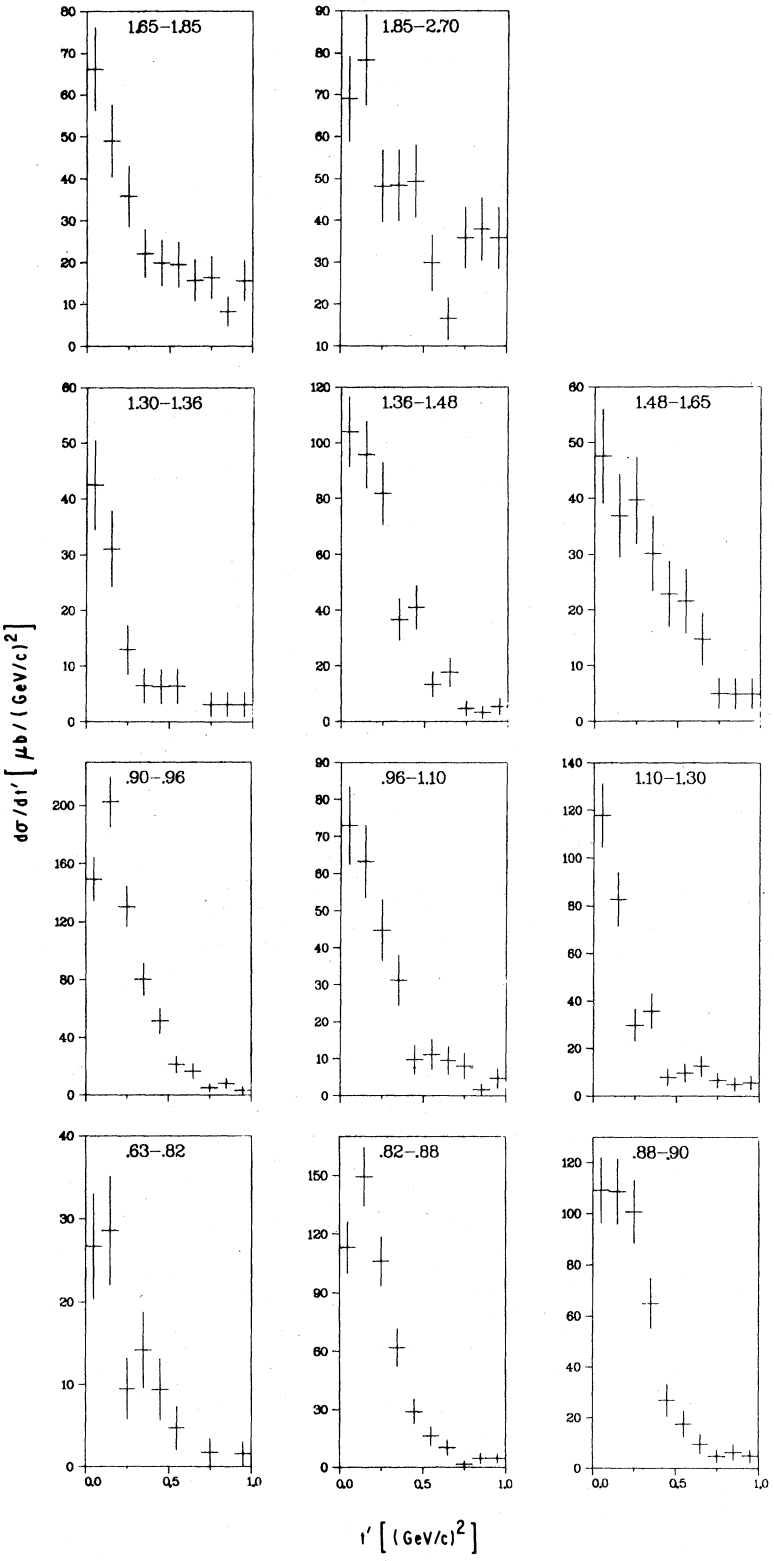

FIG. 3. t' distributions for the $\bar{K}^0\pi^-$ mass intervals indicated at the top of each distribution.

TABLE III. Results of the maximum-likelihood fit of $d\sigma/dt'$ to Eq. (2) as a function of $M(\bar{K}^0\pi^-)$ with $0.1 < t' < 1$ GeV$^2/c^2$.

Mass bin (GeV)	No. weighted events	α [(GeV/c)$^{-2}$]
0.63–0.82	46.5	4.63 ± 0.44
0.82–0.88	249.52	5.42 ± 0.20
0.88–0.90	221.2	4.61 ± 0.20
0.90–0.96	337.0	5.05 ± 0.16
0.96–1.10	120.6	3.88 ± 0.24
1.10–1.30	128.6	3.91 ± 0.24
1.30–1.36	45.4	4.24 ± 0.40
1.36–1.48	193.2	4.19 ± 0.18
1.48–1.65	112.7	2.57 ± 0.14
1.65–1.85	130.6	2.31 ± 0.13
1.85–2.58	239.8	2.08 ± 0.07

mass of the $(\bar{K}^0\pi^-)$ system increases, indicating that for larger masses, higher partial waves become important.

(b) The distribution in azimuthal angle ϕ_t shows a rough $\sin^2\phi_t$ behavior for many of the mass intervals. This suggests that the production mechanism for the $\bar{K}^0\pi^-$ system does not conserve the t channel helicity, and that probably a $\Delta m = 1$ natural-parity-exchange amplitude (which will cause such a $\sin^2\phi$ behavior) is responsible for this production mechanism.

IV. THE REACTIONS $K^-p \to K^{*-}(892)p$ AND $K^-p \to K^{*-}(1430)p$

In this section, we consider the reactions

$$K^-p \to K^{*-}(892)p\,, \tag{3}$$

$$K^-p \to K^{*-}(1430)p\,. \tag{4}$$

As in previous analyses[7], events were assigned to reactions (3) and (4) by selecting the mass of the $\bar{K}^0\pi^-$ system. We shall assume that in the mass regions selected, the spin-parity states $J^P = 1^-$ and 2^+, respectively, are dominant and that background contributions and interferences are either unimportant or show the same behavior as the resonance. Our main interest in this analysis will be the separation of the natural- and unnatural-parity-exchange mechanisms.

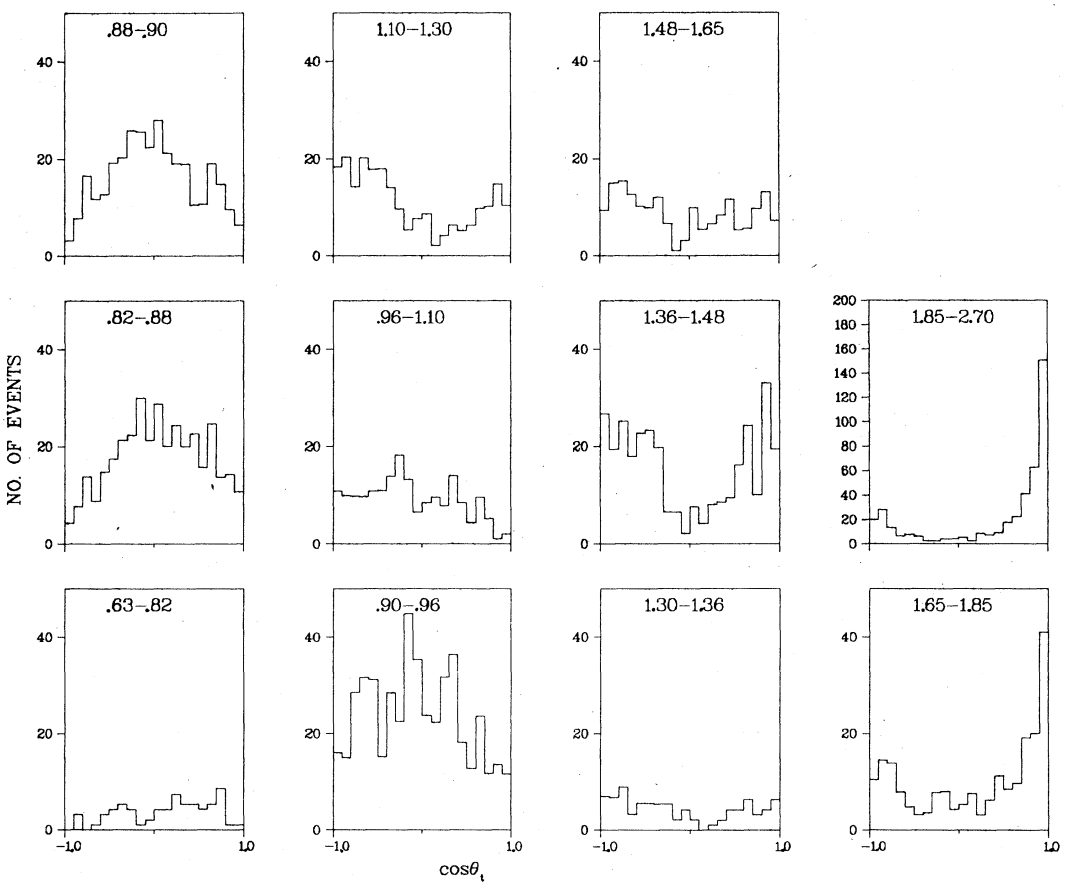

FIG. 4. $\cos\theta_t$ distribution for the same $\bar{K}^0\pi^-$ mass intervals as in Fig. 3. θ_t is the polar angle of the $\bar{K}^0$ with respect to the beam direction as measured in the $\bar{K}^0\pi^-$ rest system. Only events with $t' < 1$ (GeV/c)^2 are included.

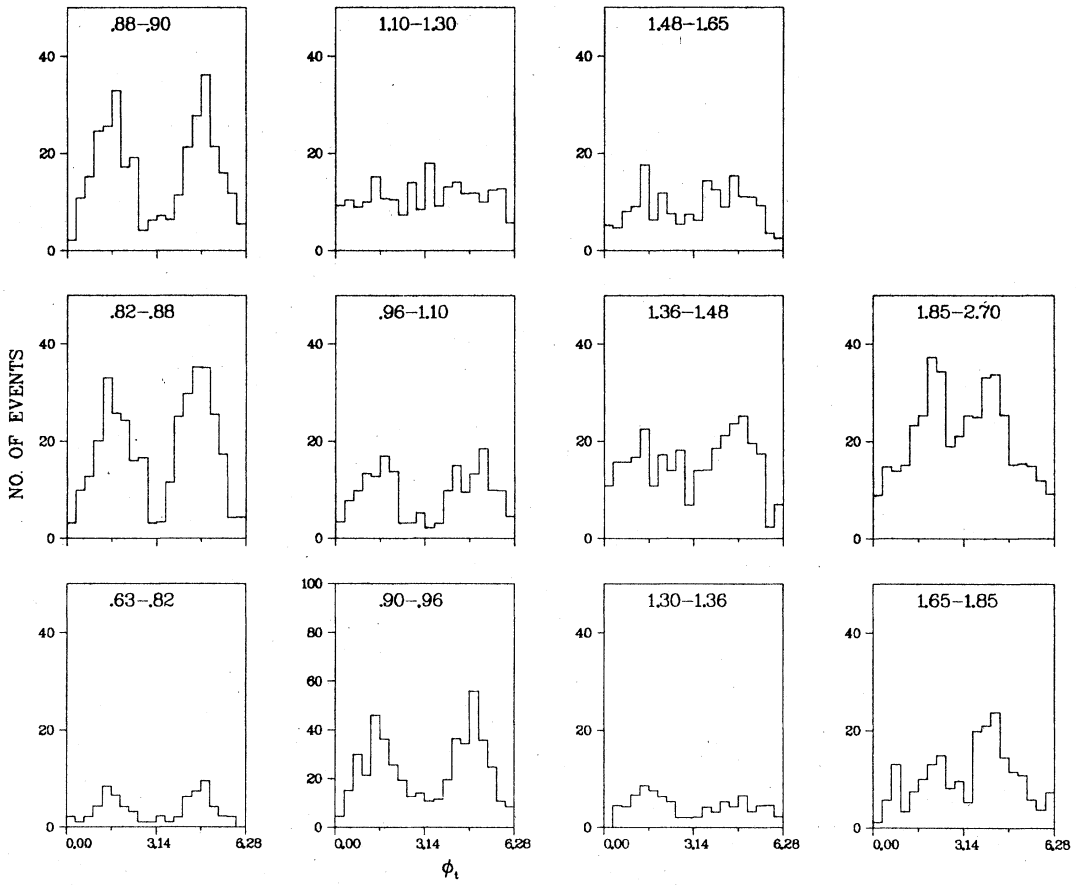

FIG. 5. Analogous distribution to that in Fig. 4 using the azimuthal angle ϕ_t rather than the polar angle θ_t.

The resonance parameters and cross sections were obtained by fitting the $\bar{K}^0\pi^-$ effective-mass distribution to three Breit-Wigner functions representing $K^*(892)$, $K^*(1430)$, and $K^*(1780)$ production, along with a cubic polynomial for the background. Results of the fit along with the relevant cross section are given in Table IV, and the fitted curve is shown in Fig. 2(c). Our results for the central value and width of the resonances are in good agreement with other published results.[8]

As may be inferred from the fit, the amount of background in the $K^*(892)$ region $[0.85 \leq M(\bar{K}^0\pi) \leq 0.95$ GeV] is very small (~8%), while the background contribution in the $K^*(1430)$ region $[1.36 \leq M(\bar{K}^0\pi) \leq 1.48$ GeV] is large (~40%). Therefore, for the differential cross section, we have subtracted the background distribution in the $K^*(1430)$ region by fitting the t' distribution in the region $1.26 \leq M(\bar{K}^0\pi^-) \leq 1.60$ GeV to a linear background and the $K^*(1430)$ resonance. However, it was not possible to make a background subtraction for the density matrix elements (and therefore the natural and unnatural parity exchanges), and so they are presented without this correction. The differential cross section $d\sigma/dt'$ for reactions (3) and (4) are given in Fig. 6 with a background subtraction applied to the $K^*(1430)$ as discussed above.

The density matrix elements $\rho_{mm'}$ were calculated using the method of moments, and are displayed in

TABLE IV. $\bar{K}^0\pi^-$ effective-mass distribution fit results. ND = 75; $\chi^2/\text{ND} = 1.21$.

Reaction	%	Central value (GeV)	Width (GeV)	Cross section (μb)
$K^- p \to K^*(890) p$	45.2 ± 2.5	0.891 ± 0.001	0.051 ± 0.002	180.8 ± 22
$K^- p \to K^*(1420) p$	10.3 ± 1.1	1.423 ± 0.005	0.085 ± 0.016	41.2 ± 6.0
$K^- p \to K^*(1760) p$	2.1 ± 0.7	1.762 ± 0.009	0.08 [a]	8.4 ± 2.9

[a] Kept fixed during fit.

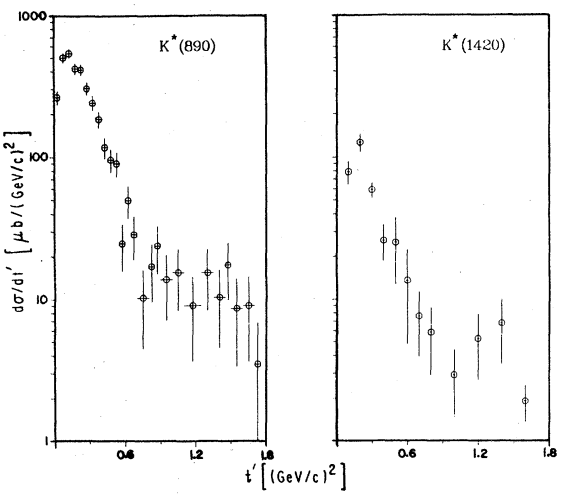

FIG. 6. $d\sigma/dt'$ for reactions (3) and (4).

Fig. 7. Using relations between density matrix elements,[7(b)] we extracted the contributions of natural parity (n) and unnatural parity (u) to the differential cross section, and these are shown in Fig. 8. We observe the following.

(a) The contribution of the $m=2$ amplitude to the $K^*(1430)$ differential cross section is compatible with zero.

(b) The contribution to the total cross section of the unnatural-parity relative to natural-parity exchange is somewhat larger for the $K^*(1430)$ than it is for the $K^*(892)$. This was observed earlier and is compatible with the expectations of a dual triple-Regge exchange model, which predicts that the ratio of π to f-ω exchange in resonance production is expected to increase linearly with the resonance mass squared.[9]

V. PARTIAL-WAVE ANALYSIS OF THE LOW-MASS $\bar{K}^0\pi^-$ SYSTEM

In order to achieve a more complete understanding of the background in the low-mass spectrum of the $\bar{K}^0\pi^-$ system, we performed a partial-wave analysis of the $\bar{K}^0\pi^-$ system for mass below 1.7 GeV.

This analysis is known to be limited in its results whenever unpolarized targets are used. In addition, although the background from other quasi-two-body reactions in other channels like $K^-p \to N^{*0}\bar{K}^0$ is small, interference effects can lead to erroneous results in high $\bar{K}^0\pi^-$ masses and large t'. Therefore, we restricted our analysis to $M(\bar{K}^0\pi^-) < 1.7$ GeV, $t' < 0.8$ (GeV/c)^2 and only consider $J \leq 2$.

The spherical harmonic moments $\langle Y_{lm} \rangle$, displayed in Fig. 9, are related to the generalized density matrix element $\rho^{JJ'}_{mm'}$ as described by the formalism of Sekulin.[10] However, since there exist many more generalized density matrix elements than spherical harmonic moments, the equations without the positivity condition are very underconstrained and thus the results of the anal-

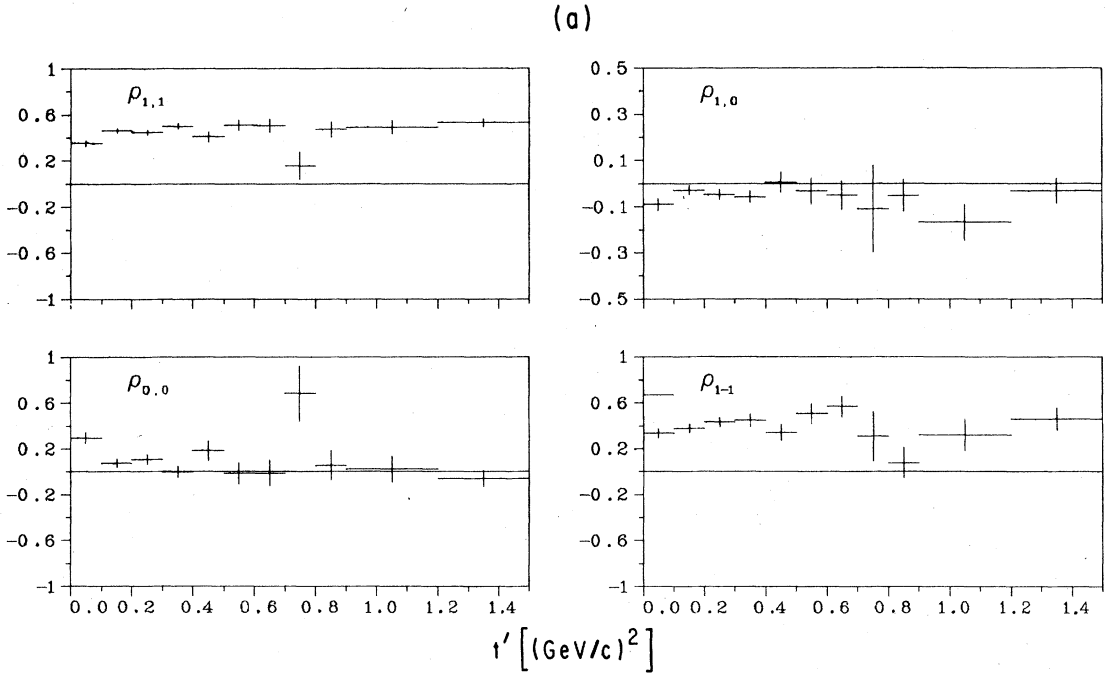

FIG. 7. $\rho_{mm'}$ distributions as functions of t' for (a) $K^-p \to K^{*-}(890)p$ and (b) $K^-p \to K^{*-}(1430)p$.

ysis are assumption-dependent. We shall assume, as in a previous analysis,[7(b)] that the contribution to the unnatural-parity-exchange mechanism is due only to pion exchange, that is, we will assume

$$\rho^{JJ'}_{mm'} + (-1)^{m'}\rho^{JJ'}_{m-m'} = 0 \qquad (5)$$

unless $m = m' = 0$. Support for this assumption comes from the fact that it leads to three relations[11] between moments of spherical harmonics that, on the average, are verified within 1.5 standard deviations.

In our analysis, we shall determine the partial cross section $\sigma(J^P m^\eta)$ for the $\bar{K}^0\pi^-$ system in J^P_m state $[P = (-1)^J]$ by an exchange of naturality η. These cross sections are related to $\rho^{JJ}_{mm'}$ by

$$\sigma(J^P m^\eta) = [\rho^{JJ}_{mm} - \eta(-1)^{|m|}\rho^{JJ}_{m-m}]\frac{d\sigma}{dM}, \qquad (6)$$

where $d\sigma/dM$ is the cross section at a specified $\bar{K}^0\pi^-$ mass.

Specifically, we shall calculate as a function of mass the following cross sections: $\sigma(1^-1^+)$, $\sigma(2^+0^-)$, $\sigma(2^+1^+)$, and $\sigma(2^+2^+)$. In addition, since the cross sections $\sigma(0^+0^-)$ and $\sigma(1^-0^-)$ cannot be separated unambiguously from each other and from the ρ^{20}_{00}

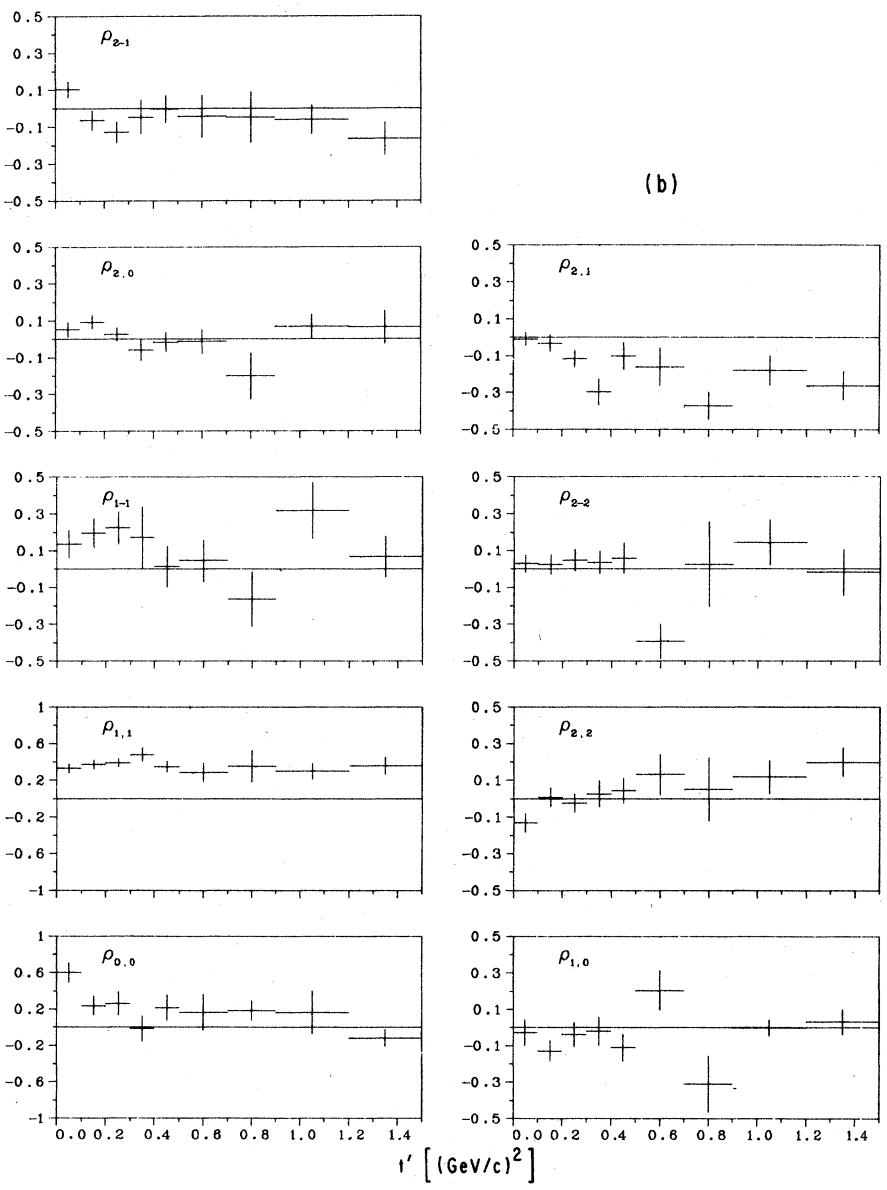

FIG. 7 *(Continued)*.

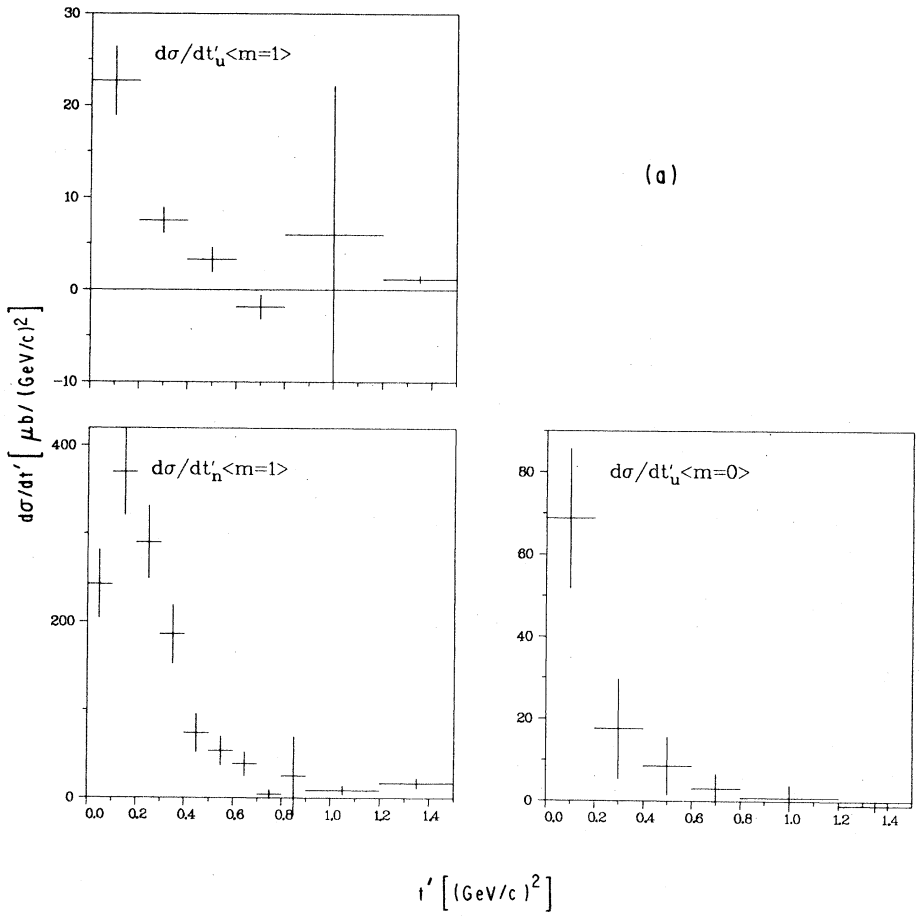

FIG. 8. Natural-parity (n) and unnatural-parity (u) partial cross sections for (a) $K^-p \to K^{*-}(890)p$ and (b) $K^-p \to K^{*-}(1420)p$.

interference term, we determined the following combinations: $\sigma(0^+0^-)+\sigma(1^-0^-)$ and $\sigma(1^-0^-)+\sqrt{5}\rho_{00}^{20} \times d\sigma/dM$. The exact relations between $\sigma(J^P m^\eta)$ are given in Ref. 7b.

For the actual calculation, we have divided the $M(\overline{K}^0\pi^-)$ mass interval (0.7–1.8 GeV) into bins of width 0.05 GeV, and in each bin have calculated all of the above six partial cross sections. Results are summarized in Fig. 10. The quoted results for masses above 1.65 GeV are not reliable because of the small $J=3$ component associated with the $K^*(1780)$ resonance.

From our partial-wave analysis, the following conclusions may be drawn.

(a) The (2^+2^-) cross section is compatible with zero (except possibly at low mass), thus showing that the $m=2$ amplitudes are negligible, as already pointed out in Sec. IV.

(b) The (2^+1^+) cross section is significantly different from zero in the $K^*(1430)$ region.

(c) The (2^+0^-) cross section, which was found previously[7(b)] to be positive and different from zero in the $K^*(1430)$ region, is compatible with zero in our analysis, but subject to rather large fluctuations.

(d) The (1^-1^+) cross section shows a pronounced peak in the $K^*(892)$ region, consistent with behavior reported previously.[7(b)]

(e) The $(0^+0^-)+(1^-0^-)$ cross section shows a peak in the $K^*(892)$ region and a broad enhancement above 1.0 GeV. The $\sigma(1^-0^-)+\sqrt{5}\rho_{00}^{20}d\sigma/dM$ cross section which contains the s-d interference term, fails to show a peak in the $K^*(892)$ region as found earlier,[7(b)] but does show a broad region (1.1–1.5 GeV) in which it is not negative and where its maximum value occurs at 1.425 GeV. If we assume, as in Ref. 7(b), that the (1^-0^-) cross section is negligible above 1 GeV, then our results support a broad s-wave (0^+0^-) enhancement centered at 1.2 GeV. In a previous analysis[7(b)] at $P_{K^-}=14.2$

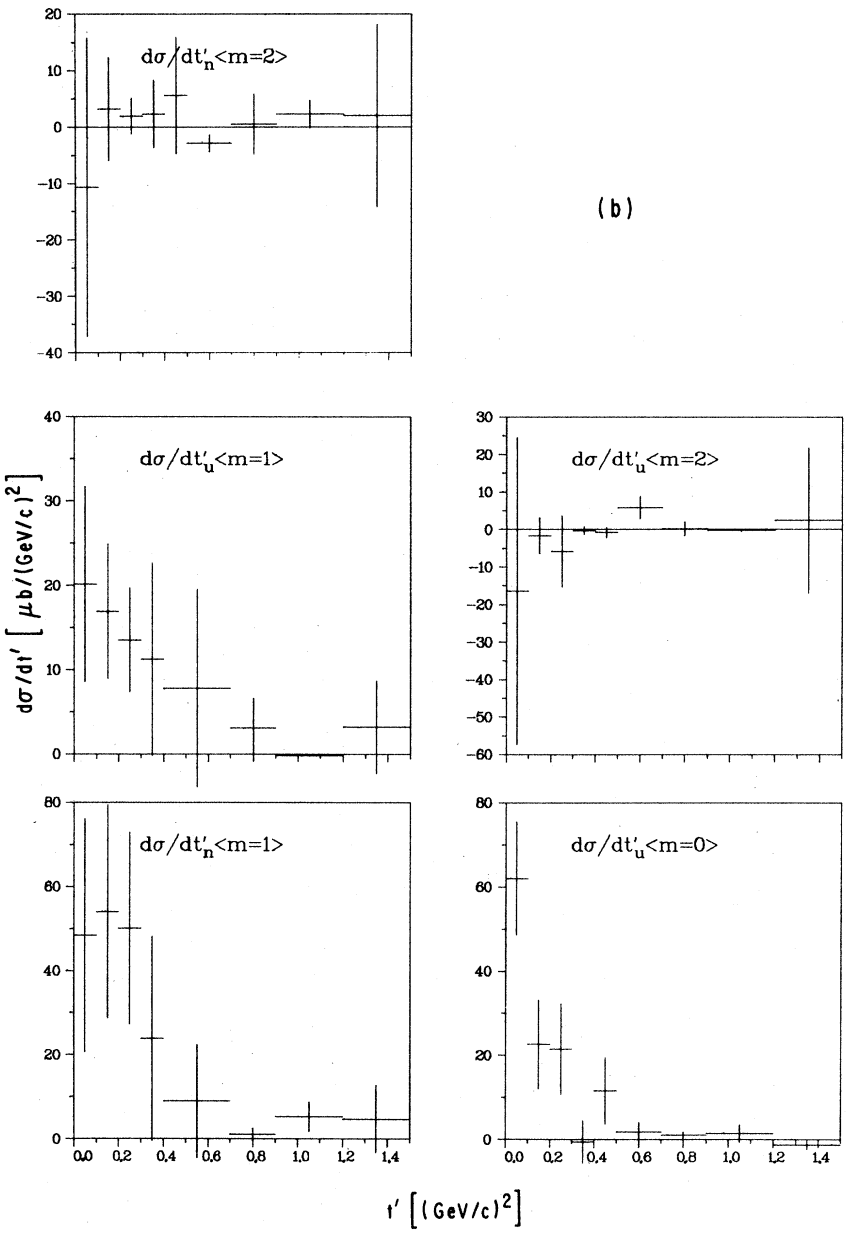

FIG. 8 *(Continued)*.

GeV/c, this enhancement was not seen in the $\bar{K}^0\pi^-$ channel. We find no indication for a narrow s-wave state above 1 GeV, in agreement with previous analysis.[7(b),12]

VI. CONCLUSIONS

We have studied K^--proton interactions in the Argonne 12-foot bubble chamber and present here some results for the reaction $K^-p \to \bar{K}^0 p\pi^-$.

The component of unnatural-parity exchange in the production of the $K^*(1430)$ is found to be larger than for the $K^*(892)$, in agreement with a triple-Regge model.[9] The partial-wave analysis reveals the presence of a broad s-wave amplitude and significant s-d and s-p interference in the region 1.1–1.5 GeV, assuming the p-wave contribution is negligible above 1 GeV. If the presence of this s wave is interpreted as being due to a resonance, its central value is 1.2 GeV and its width about 0.2 GeV.

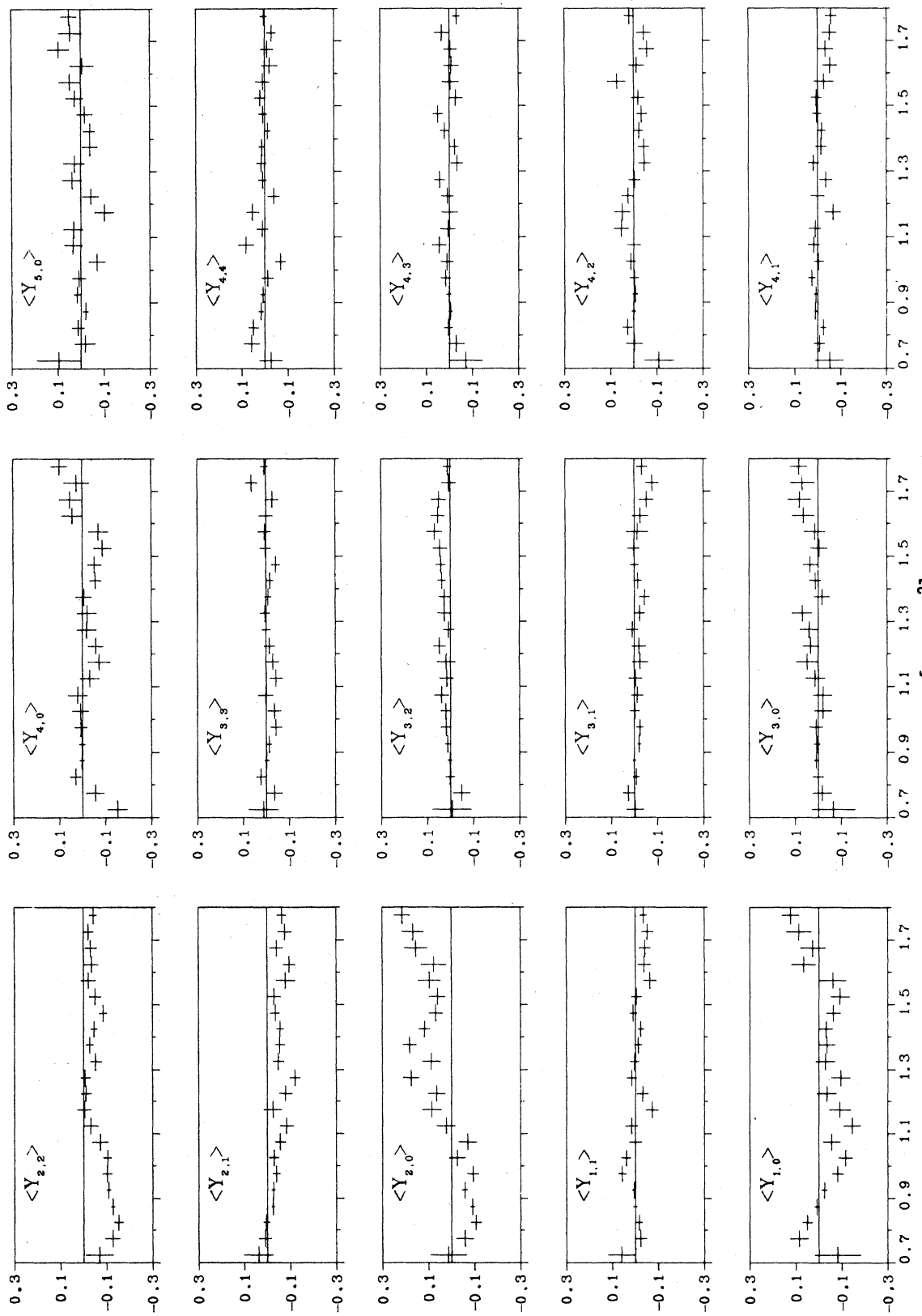

FIG. 9. $\mathrm{Re}\langle Y_{lm} \rangle$ as functions of $M(\bar{K}^0\pi^-)$ for $t' < 0.8$ $(\mathrm{GeV}/c)^2$.

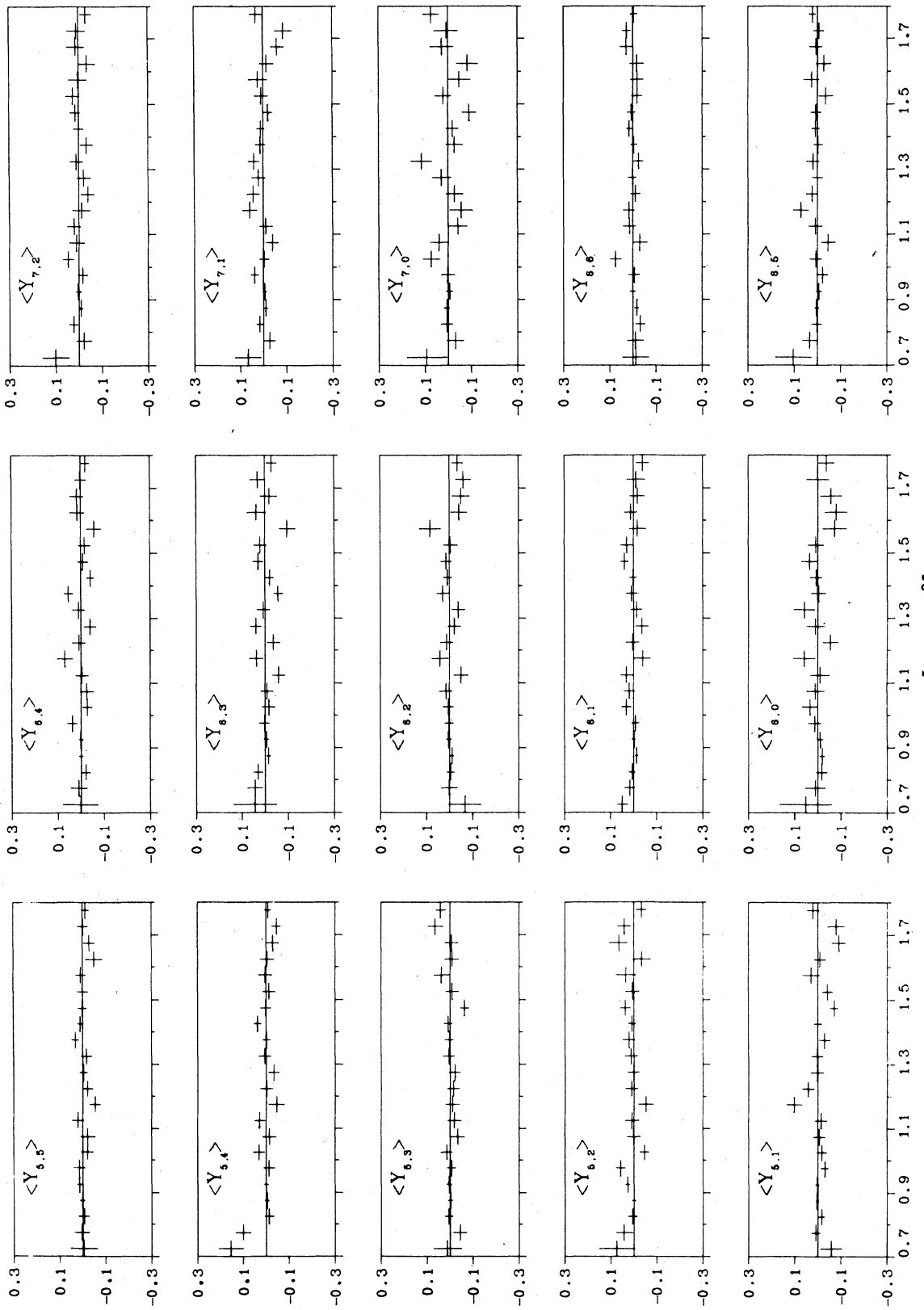

FIG. 9 *(Continued)*.

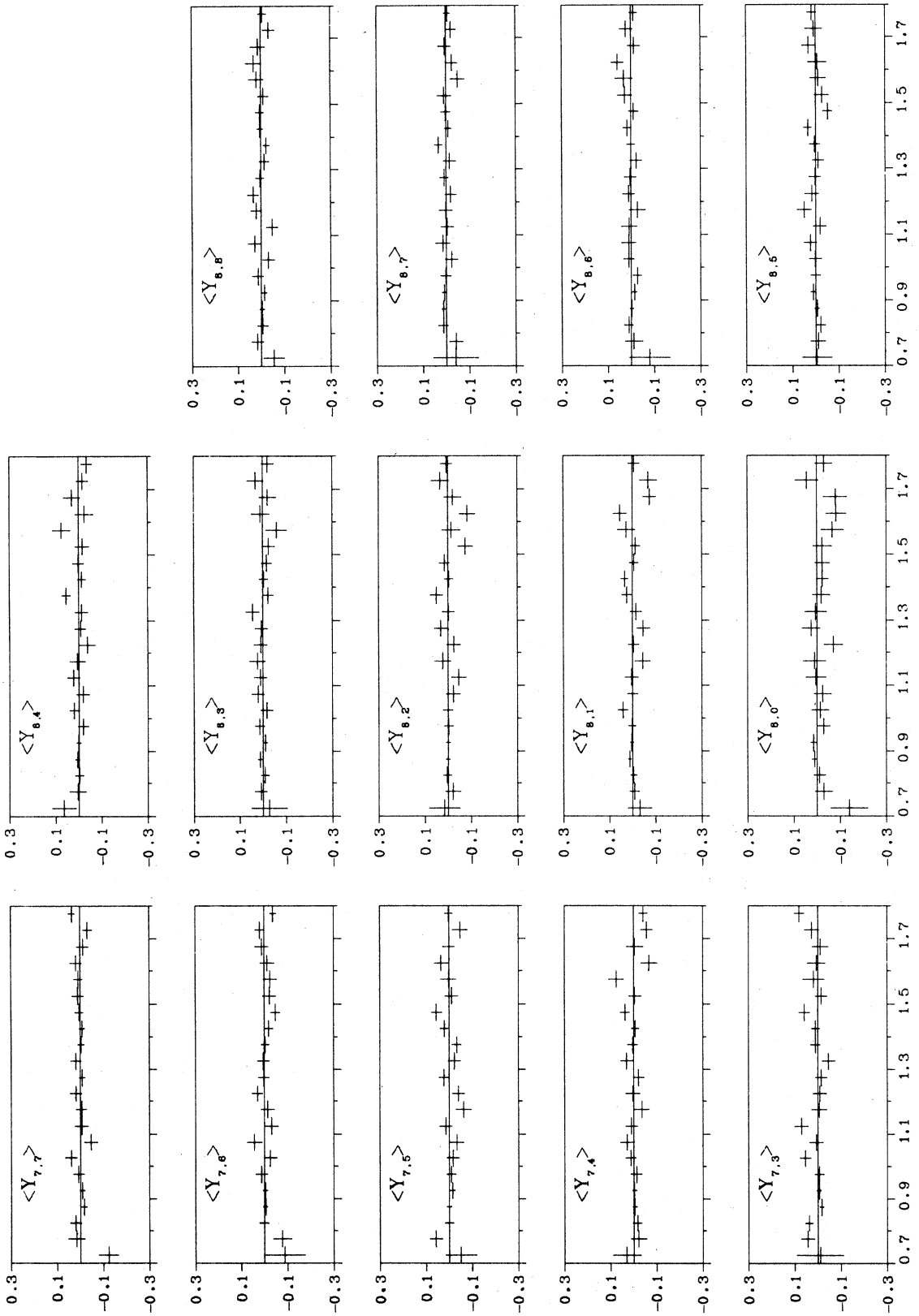

FIG. 9 (*Continued*).

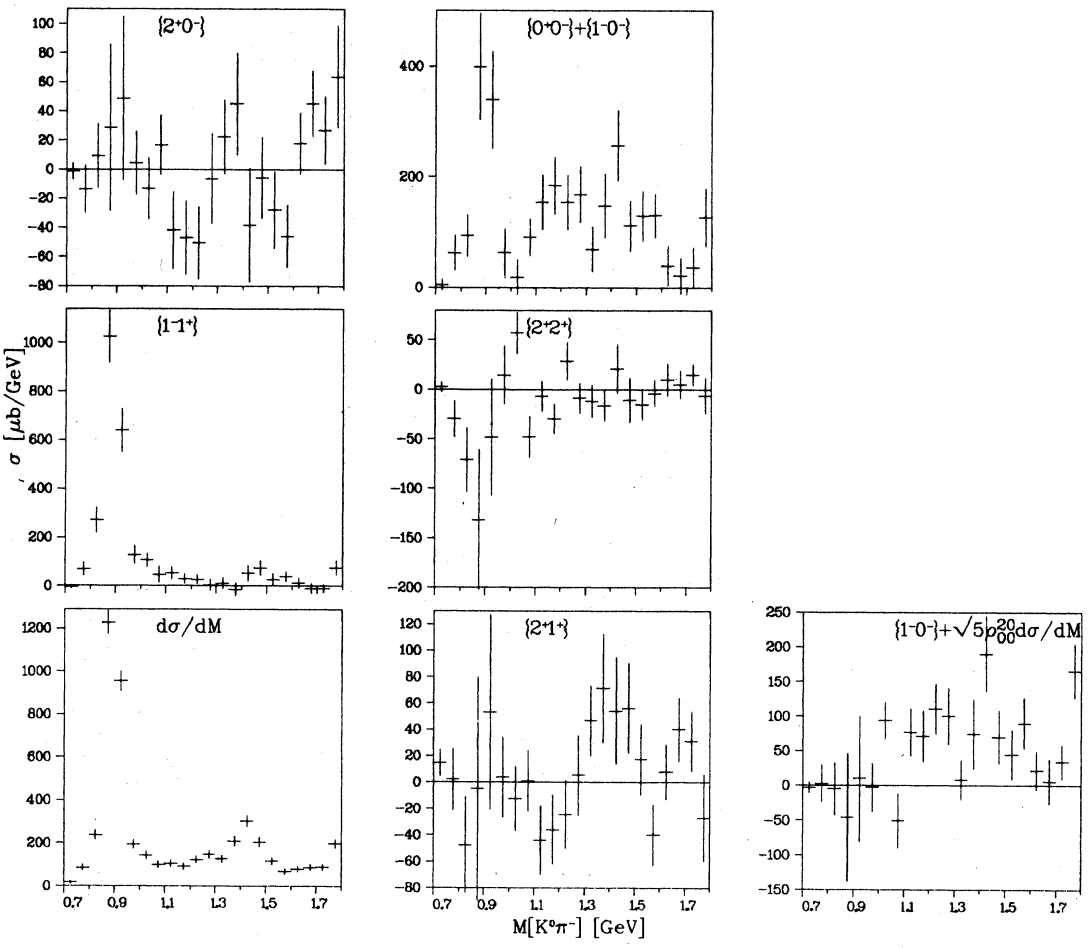

FIG. 10. $(J^P m^\eta)$ partial cross sections as functions of $M(\bar{K}^0\pi^-)$ for $t' < 0.8$ (GeV/c)^2.

ACKNOWLEDGMENTS

We would like to thank the 12-foot bubble-chamber crew and our scanning and measuring staff for their help. This work was supported by the U. S. Department of Energy and the National Science Foundation.

*On leave of absence from the Department of Physics, Technion, Haifa, Israel.

†Present address: Bell Telephone Laboratories, Naperville, Illinois 60540.

‡Present address: Max Planck Institute, Münich, Germany.

§Present address: Kaman Sciences Corp., Colorado Springs, Colorado 80907.

||Present address: S. E. Missouri State University, Cape Girardeau, Missouri 63701.

[1]R. Engelmann *et al.*, Phys. Rev. D 5, 2162 (1972); A. C. Fox *et al.*, *ibid.* 4, 2647 (1971).

[2]A. B. Wicklund *et al.*, Phys. Rev. D 17, 1197 (1978).

[3]J J. Engelen *et al.*, Nucl. Phys. B134, 14 (1978).

[4]J. Amirzadeh *et al.*, Phys. Lett. 89B, 125 (1979).

[5]C. DeClerq *et al.*, Phys. Rev. D 19, 3197 (1979); R. Riemer, Ph.D. thesis, University of Kansas, 1980 (unpublished).

[6]E. Flaminis *et al.*, Report No. CERN/HERA 70-6, 1970 (unpublished).

[7](a) F. Schweingruber *et al.*, Phys. Rev. 166, 1317 (1968); (b) M. Spiro *et al.*, Nucl. Phys. B125, 162 (1977) and references therein.

[8]Particle Data Group, Phys. Lett. 75B, 1 (1978).

[9]P. Hoyer *et al.*, Nucl. Phys. B56, 173 (1973).

[10]R. L. Sekulin, Nucl. Phys. B56, 227 (1973).

[11]The relations are Eqs (31a)–(31c) in Sekulin's paper, Ref. 10.

[12]A. Firestone *et al.*, Phys. Rev. Lett. 26, 1460 (1971).